PCCP

Ground and excited states analysis of alkali metal ethylenediamine and crown ether complexes

Journal:	*Physical Chemistry Chemical Physics*
Manuscript ID	CP-ART-06-2021-002552.R1
Article Type:	Paper
Date Submitted by the Author:	17-Aug-2021
Complete List of Authors:	Ariyarathna, Isuru; Auburn University, Chemistry and Biochemistry Miliordos, Evangelos; Auburn University, Chemistry and Biochemistry

Ground and excited states analysis of alkali metal ethylenediamine and crown ether complexes

Isuru R. Ariyarathna[†] and Evangelos Miliordos*

Department of Chemistry and Biochemistry, Auburn University,

Auburn, AL 36849-5312, USA

AUTHOR INFORMATION

Corresponding Author

*E-mail: emiliord@auburn.edu

[†]Current address: Department of Chemical Engineering, Massachusetts Institute of Technology, Cambridge, MA 02139, USA

Abstract

High-level electronic structure calculations are carried out to obtain optimized geometries and excitation energies of neutral lithium, sodium, and potassium complexes with two ethylenediamine and one or two crown ether molecules. Three different sizes of crowns are employed (12-crown-4, 15-crown-5, 18-crown-6). The ground state of all complexes contains an electron in an *s*-type orbital. For the mono-crown ether complexes, this orbital is the polarized valence *s*-orbital of the metal, but for the other systems this orbital is a peripheral diffuse orbital. The nature of the low-lying electronic states is found to be different for each of these species. Specifically, the metal ethylenediamine complexes follow the previously discovered shell model of metal ammonia complexes (1s, 1p, 1d, 2s, 1f), but both mono- and sandwich di-crown ether complexes bear a different shell model partially due to their lower (cylindrical) symmetry and the stabilization of the 2*s*-type orbital. Li(15-crown-5) is the only complex with the metal in the middle of the crown ether and adopts closely the shell model of metal ammonia complexes. Our findings suggest that the electronic band structure of electrides (metal crown ether sandwich aggregates) and expanded metals (metal ammonia aggregates) should be different despite the similar nature of these systems (bearing diffuse electrons around a metal complex).

1. Introduction

Electrides are solids that contain trapped electrons in their cavities or pores.[1, 2] The pioneering work of Dye and co-workers in early 1980's disclosed the existence of these materials by separating a Cs^+ core from its valence electron using crown ethers. Specifically, two 18-crown-6 (18C6) crown ethers coordinate to each Cs^+ ion and the electrons diffuse in the periphery of these complexes residing in the formed cavities. [3, 4] Since then, numerous systems have been examined termed as either organic (metal complexes with crown ethers or cryptands)[5-10] or inorganic (such as $[Ca_{24}Al_{28}O_{68}]^{4+}@4e^-$).[11, 12] A different category of inorganic electrides composed of cationic crystal and anionic electron layers has also been discovered, such as the two-dimensional Ca_2N and other nitride systems.[13-15] Various applications have been reported in the literature including CO_2 activation,[16] ammonia synthesis,[17, 18] and organic synthesis.[19, 20] Computational studies have largely contributed to understanding the properties of these materials. The periodic density functional theory calculations of the Johnson group have shed light to their stability and electronic, magnetic, and chemical properties. [21-27]

The complexation of positively charged alkali metals with crown-ethers (CE) finds applications in the selective isolation or extraction of the metal ions from solutions.[28-30] For this reason different mono and di-CE complexes with pure or "functionalized" (addition of side chains) CE have been studied in the literature.[31-34] The same concept has been applied in 2D-materials, where a CE-type hole is incorporated in the graphene sheet.[35-37] These complexes are also introduced in new materials.[33, 38, 39] We are aware of only one recent study on neutral alkali metal-CE complexes [Li(12-crown-4) or Li(12C4), Na(15-crown-5) or Na(15C5), K(18-crown-6) or ~~or~~ K(18C6)] which explains the lower ionization of the ground state of these complexes with respect

to the metal atom.[40] A systematic electronic structure study on more complexes (in their ground and excited states) and their connection to electrides is still missing.

Metal ammonia complexes have been shown to form crystalloid structures with a grid of positively charged metal ammonia complexes and "free" diffuse electrons orbiting among them.[41-52] These materials (termed as expanded or liquid metals) have metallic properties and have been proposed as high-temperature superconducting materials.[53] The similarity of electrides and expanded metals has been expressed in the literature.[54] Experimentally only alkali and alkaline earth metals have been investigated but theoretical studies demonstrated that transition metals can form identical structures.[55-57]

Inspired by the rising interest on expanded metals, our research group has recently published a series of articles on the electronic and geometric structure of their building units.[55-66] Ground and low-lying excited electrons states have been studied for metal ammonia complexes via high-level electronic structure methodologies. We have shown that diffuse electrons reside in the periphery of positively charged metal ammonia complexes occupying hydrogenic-type orbitals. The Aufbau principle (1s, 1p, 1d, 2s, 1f, 2p) resembles that of the Jellium or nuclear shell models, which describe approximately the electronic structure of small metallic particles (superatoms)[67] and the proton/neutron shell model within nuclei.[68] Transition metals maintain their inner d-shell in addition to the outer peripheral orbitals, and the inner electrons act nearly independently of the outer ones.[65]

Besides ammonia, other solvents or molecular scaffolds, such as water, ethers, methylamine, tetrahydrofuran, and dodecahedrane have been shown to solvate electrons and form solvent separated ions-electrons.[41, 43, 69-86] Presently, we investigate the electronic structure of neutral metal crown ether complexes by means of high-level quantum chemical techniques.

Specifically, we combine lithium, sodium and potassium with three differently sized crown ethers (12C4, 15C5, 18C6). Experimentally synthesized electrides combine Li through Cs alkali metals with 18C6, 15C5 crown ethers, and cryptands ("polycyclic crown ethers"). Presently, our goal is to perform a systematic study on metal-crown ether complexes with one or two crowns, study their stability, show that these systems (shown in Figure 1) can accommodate outer diffuse electrons, identify the nature of the excited states and the orbital series of these systems, and monitor how the excitation energies change with the metal identity and the ether size. In addition, we include the study of metal-ethylenediamine (see Figure 1) complexes as a bridge between the building units of organic electrides and expanded metals.

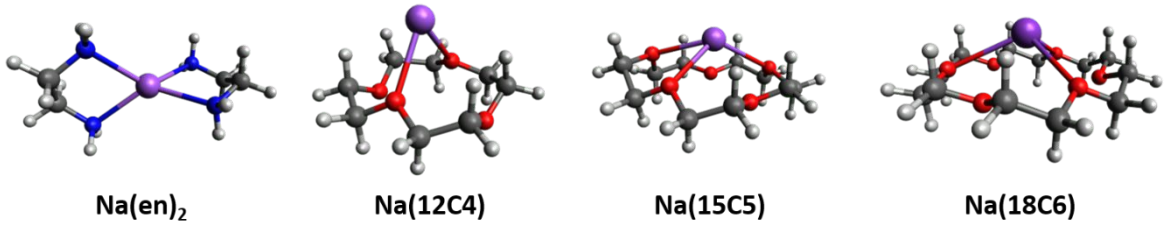

Figure 1. Typical geometries of the examined metal-ethylenediamine and metal-crown-ether molecules.

2. Computational Details

$M(en)_2$, M(12C4), M(15C5) [M = Li, Na, K], and M(18C6) [M = Na, K] structures were optimized at the second-order Møller–Plesset perturbation theory (MP2).[87] At the same level of theory binding energies (D_e) were obtained with respect to M + 2 (en) and M + 12C4/15C5/18C6 fragments. The spin contamination for the unrestricted Hartree−Fock wavefunction of these species is minor. D_e values of $M(en)_2$ and M(12C4) [M = Li, Na] were also evaluated by performing CCSD(T) (coupled-cluster singles, doubles, and perturbative triples) [88-91] calculations at the MP2 optimized geometries (CCSD(T)//MP2). Only valence electrons are correlated at MP2

and CCSD(T). Harmonic vibrational frequencies were obtained at DFT/B3LYP (DFT ≡ Density Functional Theory) [92, 93] level to confirm that every structure is a minimum of the potential energy surface and obtain zero-point energy (ZPE) corrections. For MP2, CCSD(T), and DFT calculations the cc-pVTZ (≡TZ) basis set [94-96] is used for all atoms except hydrogens, where a series of diffuse functions (aug-cc-pVTZ ≡ ATZ) [97] has been added to describe the peripheral orbitals more accurately.[58] In the case of Li(12C4) we also explored the effect of diffuse functions on the lithium center (ATZ).

The MP2 optimized ground state geometries were used for the excited state calculations. Koopmans's theorem (KT), diagonal second-order (D2), partial third-order quasiparticle method (P3), and renormalized partial third-order quasiparticle (P3+) electron propagator theory (EPT) [98-101] methods were used to calculate vertical electron attachment energies of the corresponding cations. Vertical excitation energies of the neutral molecules were inferred from the differences of the calculated electron attachment energies. The accuracy increases in the KT < D2 < P3 < P3+ order. In all cases, the pole strengths are higher than 0.9 validating the use of EPT. Vertical electron attachment energies and pole strengths are reported in the Electronic Supplementary Information (ESI). Several low-lying excited states of the smallest $Li(en)_2$ were further investigated at the EOM-EA-CCSD (equation-of-motion coupled-cluster method for the electron affinity) theory. [102-105] The basis set of hydrogen has been enhanced with an additional series of diffuse functions for the excited state calculations, d-aug-cc-pVTZ (≡DATZ) for $M(en)_2$ and M(12C4). For the larger complexes, M(15C5) and M(18C6), we had to reduce the basis set to double-ζ quality: cc-pVDZ for all atoms and d-aug-cc-pVDZ for hydrogen.[106]

The geometry optimization of the $M(12C4)_2$ complexes was carried out at the CAM-B3LYP/cc-pVTZ(C,O) aug-cc-pVTZ(H) level of theory, and the excited states of $K(12C4)_2$, which is the only one making a sandwich structure, at EPT/cc-pVDZ(C,O) d-aug-cc-pVDZ(H).

Gaussian 16 suite [107] was used for the MP2, DFT, and EPT calculations. CCSD(T) and EOM-EA-CCSD calculations were carried out with MOLPRO 2015.1 [108] and Q-CHEM5.1 [109] packages, respectively. Molden [110, 111] and GaussView [112] software was used create Dyson orbital plots.

3. Results and Discussion

$M(en)_2$. The complexation of the two ethylenediamine molecules to Li, Na, and K creates a pseudo-tetrahedral (D_2) geometry with four equivalent M−N bonds. The M−N bond length scales linearly with the size of the metal. There is an excellent linear correlation ($R^2 = 0.9994$) between the M−N bond length (see Table 1) and the covalent radius of the metal (1.30, 1.60, and 2.00 Å for Li, Na, and K, respectively).[113] The Li−N and Na−N distances of $M(en)_2$ are longer than those of $Li(NH_3)_4$ and $Na(NH_3)_4$ by 0.003 and 0.033 Å (CCSD(T) level)[59] and by 0.002 and 0.027 Å (current MP2 values for $Li(NH_3)_4$ and $Na(NH_3)_4$ = 2.079 and 2.483 Å), and the total binding energies D_e decrease by ~10 kcal/mol (or ~2.5 kcal/mol per bond; current MP2 values for $Li(NH_3)_4$ and $Na(NH_3)_4$ are 54.9 and 30.1 kcal/mol). The MP2 and CCSD(T)//MP2 D_e values of Table 1 agree within 2 kcal/mol validating the accuracy of our MP2 values for the rest of the complexes. Going from Li to Na, we see that D_e drops to about half (44.8 vs. 19.9 kcal/mol) but only a quarter going from Na to K (19.9 vs. 15.0 kcal/mol). This is due to the smaller charge density (charge/volume) of the heavier metals. Finally, the vertical ionization energy of the $M(en)_2$ complexes is practically independent of the central metal and equal to 2.45−2.48 eV (see Table 1),

which is considerably smaller than the ionization energy of the plain metals (see Table 1). The ionization energy of $Li(NH_3)_4$ and $Na(NH_3)_4$ is slightly larger (2.92 and 2.79 eV)[59] probably because of the screening of the metallic charge to the outer electron caused by the carbon chains of $M(en)_2$. As shown in Figure 2, the outer orbital is distributed evenly around the $Li(NH_3)_4^+$ core but it is polarized away from the carbon chains of the $Li(en)_2^+$ core.

The excited states of $M(en)_2$ follow the same pattern as in $M(NH_3)_4$. Table 2 lists the computed excitation energies and Figure 3 depicts the corresponding Dyson orbitals. The first three excited states are of 1p character spanning an energy range of 0.258, 0.265, and 0.261 eV for M = Li, Na, K, respectively. The higher symmetry of $M(NH_3)_4$ places all three 1p components together at 0.72 and 0.66 eV for M = Li and Na.[59] These values are higher than the excitation energy of all three 1p excitations of $M(en)_2$ (see Table 2) indicating again that the nuclear charge is screened by the carbon chains. The average 1p excitation energies for $M(en)_2$ are 0.46, 0.48, and 0.54 eV for M = Li, Na, and K revealing a slightly increasing excitation energy as we move to larger metals. This is the opposite trend observed for $M(NH_3)_4$, M = Li, Na (see above), where the excitation energy drops from 0.72 to 0.66 eV.[59] The next group of states has 1d character, but the five components span a smaller energy range of about 0.1 eV (see Table 2) and they lie 1.0-1.1 eV higher than 1s state for all three metals. The 2s state follows next at ~1.4 eV and the 1f states come next in the 1.40-1.65 eV range. The Dyson orbitals suggest a mixed character of 2p, 1g, and 2d orbitals and are given in the Figures S1, S2, and S3 of the ESI. We have calculated all the bound states of these systems with respect to the ionization $M(en)_2^+ + e^-$ limit. The highest four are actually above it at the lower KT level but below it at every other level (D2, P3, P3+). According to Table 2, the excitation energies increase by 0.1 eV or more going from KT to D2. The D2 values have practically converge with respect to P3, P3+ or EOM-EA-CCSD approaches.

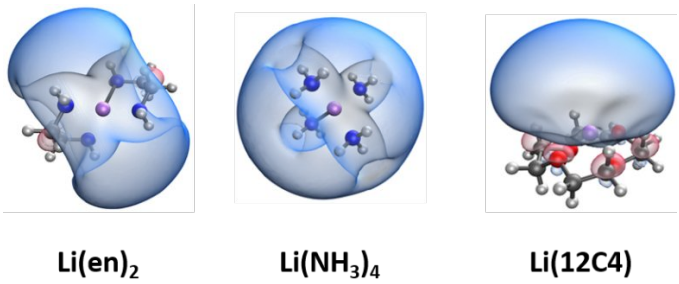

Figure 2. Contours of the singly occupied outer orbital of $Li(en)_2$, $Li(NH_3)_4$, and Li(12C4). An iso-value of 0.03 $Å^{-3}$ was used.

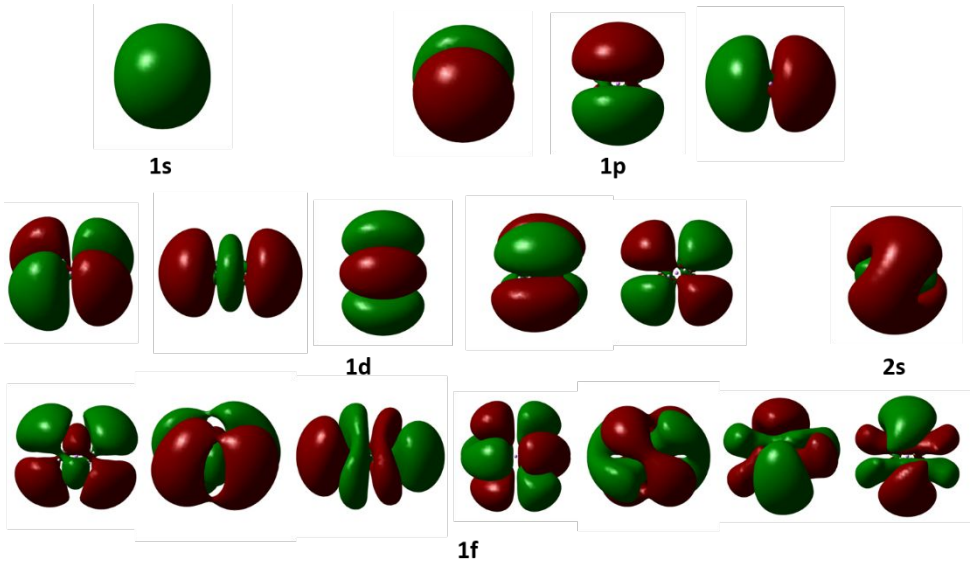

Figure 3. Select Dyson orbitals for the $Li(en)_2^+ + e^- \rightarrow Li(en)_2$ process. An iso-value of 0.02 $Å^{-3}$ was used.

Table 1. MP2 total binding energy (D_e and D_0, kcal/mol), P3+ and CCSD(T) vertical ionization energies (IE, eV), and MP2 equilibrium distances (r_e, Å) of the studied molecules.[a]

Species	D_e		D_0 [b]	IE		r_e		
	MP2	CCSD(T)	MP2	P3+	CCSD(T)	M−A [c]	M−X [d]	O−X [e]
$Li(en)_2$	44.8	46.7	41.4	2.48	2.57	2.081		
$Na(en)_2$	19.9	21.6	18.2	2.45	2.57	2.510		
$K(en)_2$	15.0		14.0	2.45		3.033		
Li(12C4)	18.7	19.9	16.9	2.54	2.66	2.06 (2), 2.09 (2)	0.98	1.82
Na(12C4)	5.8	6.9	5.0	3.61	3.65	2.58 (2), 3.70 (2)	2.52	1.93
K(12C4)	3.7		3.0	3.23		3.21 (2), 4.22 (2)	3.22	1.93
Li(15C5)	21.2		19.1	1.96		2.09, 2.14 (2), 2.26 (2)	0.02	2.18
Na(15C5)	12.3		10.6	2.58		2.62, 2.65, 2.66, 2.72, 2.81	1.40	2.30
K(15C5)	9.6		8.0	2.58		3.06, 3.16, 3.19, 3.26, 3.38	2.20	2.33
Na(18C6)	15.9		15.1	2.35		2.83 (2), 2.96 (2)	0.86	2.76
K(18C6)	17.2		16.0	2.33		3.12 (2), 3.25 (2)	1.49	2.82

[a] P3+ vertical ionization energies obtained with cc-pVTZ (M,C,N,O) d-aug-cc-pVTZ (H). All other results are obtain with cc-pVTZ (M,C,N,O) aug-cc-pVTZ (H).

[b] ZPE is obtained at the B3LYP level of theory (see Section 2).

[c] A is N for $M(en)_2$ or O for M(12C4), M(15C5), and M(18C6), and M = Li, Na, or K. Values in parenthesis show the number of such distances.

[d] X is the center of the crown-ether ring calculated as the center of mass of the oxygen atoms, and M−X is its distance from the metal M.

[e] Average O−X distance; see footnote *d* for the definition of X.

Table 2. Vertical excitation energies (eV) for $Li(en)_2$ at the KT, D2, P3, P3+, and EOM-EA-CCSD levels of theory.

Config. [a]	KT	D2	P3	P3+	EOM-EA-CCSD
			$Li(en)_2$		
1s	0.000	0.000	0.000	0.000	0.000
1p	0.262	0.355	0.350	0.350	0.369
	0.310	0.422	0.416	0.416	0.436
	0.483	0.613	0.607	0.608	0.621
1d	0.809−0.854	1.017−1.087	1.010−1.079	1.011−1.079	1.046−1.127
2s	1.205	1.384	1.387	1.386	1.419
1f	1.231−1.397	1.466−1.643	1.462−1.640	1.462−1.640	1.477−1.700
2p/1g/2d [b]	1.347−2.250	1.670−2.470	1.665−2.464	1.665−2.464	
			$Na(en)_2$		
1s	0.000	0.000	0.000	0.000	
1p	0.279	0.382	0.376	0.376	
	0.320	0.439	0.433	0.434	
	0.517	0.645	0.641	0.641	
1d	0.811−0.837	0.996−1.089	0.990−1.083	0.991−1.083	
2s	1.174	1.353	1.356	1.356	
1f	1.184−1.345	1.407−1.635	1.404−1.633	1.405−1.633	
2p/1g/2d [b]	1.375−2.251	1.664−2.456	1.662−2.451	1.662−2.451	
			$K(en)_2$		
1s	0.000	0.000	0.000	0.000	
1p	0.362	0.455	0.451	0.451	
	0.353	0.468	0.467	0.468	
	0.616	0.710	0.711	0.712	
1d	0.843−0.903	0.997−1.112	0.996−1.110	0.996−1.110	
2s	1.167	1.361	1.364	1.365	
1f	1.188−1.391	1.399−1.640	1.400−1.642	1.400−1.642	
2p/1g/2d [b]	1.534−2.217	1.705−2.390	1.711−2.390	1.711−2.390	

[a] Occupied orbital of each electronic state; see Figure 2. A more detailed list of excitation energies and more Dyson orbitals are given in Tables S10, S11, and S12 and Figure S1, S2, and S3 of ESI.

[b] Mixed character. The four highest energy states are not bound with respect to the ionization energy at KT level of theory.

M(12C4), M(15C5), M(18C6). Typical geometries of these systems are shown in Figure 1. The metal resides on the top of the crown ether ring, and the distance of the metal from the center of the crown ether depends on the size of the metal atom and the radius of the ring. In Table 1, we consider the center of the crown ether as the center of mass of its oxygen atoms (X) and the radius of the ring as the average O-X distance. As expected, the distance of the metal from X increases with the metal size and decreases with the ring radius. The longest M-X distance is 3.22 Å for K(12C4), while Li sits practically at the center of 15C5. In Table 1, we also list the M-O distances for each case. Two kinds of M-O distances are observed: the shorter ones between the metal and the oxygen atoms pointing to it, and the longer ones between the metal and the rest of the oxygen atoms pointing towards the opposite side of the ring. For 12C4 and 18C6, the M-O distances within each group are exactly equal (C_{2v} and C_{3v} point groups), unlike the lower symmetry 15C5 systems (C_1 point group).

The approach and anchoring of the metal to the crown ether is a result of the polarization of the valence s-orbital of the metal away from the ring (see Figure 2). The induced positively charged side of the metal is electrostatically attracted by the crown oxygen atoms. The resulting binding energies are as low as 3.7 kcal/mol for K(12C4) and as large as 21.2 kcal/mol for Li(15C5). After ZPE corrections these values drop to 3.0 and 19.1 kcal/mol (see Table 1). Generally, Li makes strong complexes and tends to reside in the middle of the ring. On the other hand, heavier metals prefer larger rings, which explains the composition (Cs and 18C6 ring) of the experimentally observed electrides.[3, 4]

Another effect of the observed bonding is the reduction of the ionization energy (IE) of the systems. The IEs of the single Li, Na, and K atoms are 5.392, 5.139, and 4.341 eV, respectively,[113] which drop to 2.54, 3.61, and 3.23 eV for Li(12C4), Na(12C4), and K(12C4). The bigger rings

enable stronger binding between the metal and the ring, which indicates a larger polarization of the valence s-orbital of the metal and thus easier ionization. Indeed, the IEs drop significantly (more than 0.5 eV) going to 15C5 systems and by ~0.25 eV going to 18C6 (see Table 1). An interesting observation is that although the IE of the single metal atoms decreases monotonically from Li to K, the IE of the Li-crown-ether complexes are significantly lower as a result of the stronger binding with the crown-ether rings. Our vertical IEs are within the DFT (PBE0, TPSSh) range of ref. [40].

We next examine the excited states of these systems, and we first focus on Li(12C4). The vertical excitation energies and the populated orbitals for all bound electronic states of Li(12C4) are given in Table 3 and Figure 4. The Dyson orbitals indicate a mixed Li-valence and crown-ether Rydberg character. For this reason, we examined two series of basis sets. The first one consists of plain TZ functions on all atoms and DATZ on hydrogen atoms. This has been successfully used for highly excited states of metal-ammonia complexes.[58, 114] The second series includes additional diffuse functions on the metal (ATZ). The excitation energies of the two series differ by no more than 0.02 eV in all cases except for two cases where the difference is larger but smaller than 0.05 eV (see Table 3). Therefore, we used the TZ/DATZ combination for the rest of the systems to compromise accuracy and efficiency.

The lowest energy states of Li are ^{2}S($1s^2 2s^1$), ^{2}P($1s^2 2p^1$), ^{2}S($1s^2 3s^1$), ^{2}P($1s^2 3p^1$), ^{2}D($1s^2 3d^1$). The ground state is well separated from the first excited state, which is 1.85 eV higher and the next three states lie closer to each other in the 3.37−3.88 eV range.[113] As stated earlier, the ground state of Li(12C4) bears an unpaired electron in a polarized 2s orbital of Li. The singly occupied orbital in the second and third excited states is a *p*-type orbital (p_x and p_y; $13b_1$ and $13b_2$ of Figure 4) diffuse in the periphery of the $Li(12C4)^+$ core and perpendicular to the Li-X axis (≡z-axis). These

two states are at 0.656 and 0.760 eV (see Table 3), clearly lower than the $2p^1$ state of lithium. The first and fourth excited states at 0.590 and 1.033 eV have an electron in one of two sp hybrids ($18a_1$ and $19a_1$) orthogonal to each other (see Figure 4). The lower energy hybrid has a larger metallic character as opposed to the higher energy hybrid, which is polarized towards the ring side. We think that the hybridization occurs between the remaining p_z-type orbital and a Rydberg *s*-type orbital. This second *s*-type orbital is higher in energy in the metal-ammonia complexes and Li(15C5); see below. The next five states have *d*-orbital character ($10a_2$ through $21a_1$) lying between 1.109 and 1.359 eV. As stated for the *p*-orbitals, these outer *d*-orbitals are much lower than the 3*d* atomic orbitals of lithium. The last five states examined presently are of *f*-orbital nature ($15b_1$ through $16b_2$), but we were not able to identify the missing two *f*-orbitals, which appear to be highly mixed with other diffuse molecular orbitals (see ESI for more states and Dyson orbitals). Conclusively, the metal complexes with a single crown ether ligand resemble the supatomic nature observed for metal-ammonia complexes (see Introduction) with similar excitation energies (±0.2 eV; compare for example Tables 2 and 3), except for the 2s orbital which has lower energy in the crown ether case.

Table 3. Vertical excitation energies (eV) for Li(12C4) at the KT, D2, P3, and P3+ levels of theory. Two series of basis sets are employed for P3+. The states are ordered according to P3+ excitation energies.

Config. [a]	KT [b]	D2 [b]	P3 [b]	P3+ [b]	P3+ [c]
$17a_1$	0.000	0.000	0.000	0.000	0.000
$18a_1$	0.421	0.609	0.587	0.590	0.589
$13b_1$	0.488	0.681	0.654	0.656	0.657
$13b_2$	0.557	0.786	0.758	0.760	0.760
$19a_1$	0.819	1.048	1.031	1.033	1.032
$10a_2$	0.869	1.135	1.106	1.109	1.109
$20a_1$	0.881	1.155	1.126	1.129	1.126
$14b_1$	0.873	1.161	1.136	1.138	1.138
$14b_2$	0.894	1.182	1.157	1.159	1.158
$21a_1$	1.136	1.385	1.374	1.375	1.359
$15b_1$	1.308	1.612	1.592	1.594	1.560
$16b_1$	1.296	1.639	1.613	1.615	1.616
$15b_2$	1.295	1.641	1.614	1.617	1.617
$11a_2$	1.327	1.691	1.667	1.669	1.669
$16b_2$	1.356	1.712	1.690	1.692	1.673

[a] Occupied orbital of each electronic state; see Figure 4. A more detailed list of excitation energies and more Dyson orbitals are given in Table S13 and Figure S4 of ESI.

[b] The DATZ basis set is used for hydrogen and TZ for all other atoms.

[c] The DATZ basis set is used for hydrogen, ATZ for lithium, and TZ for all other atoms.

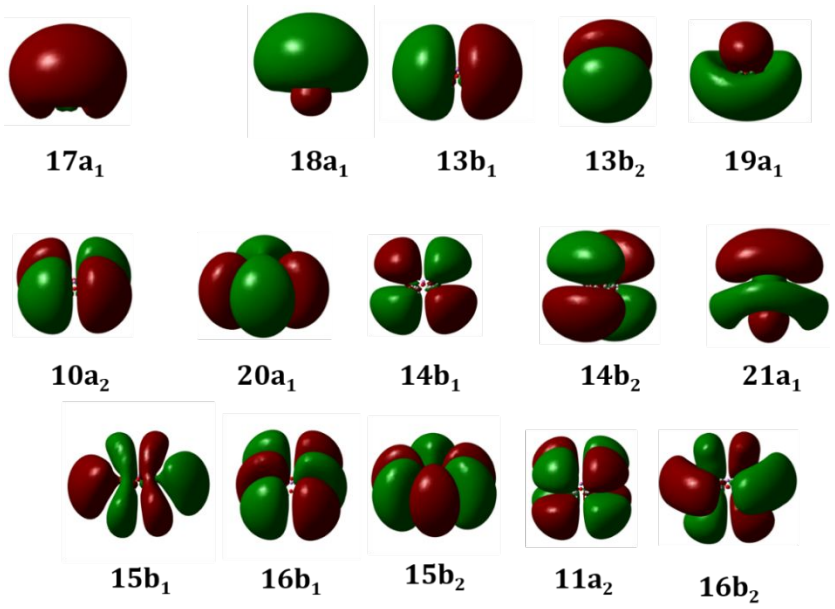

Figure 4. Select Dyson orbitals for the $Li(12C4)^+ + e^- \rightarrow Li(12C4)$ process. Li is on the top of the crown ether. An iso-value of 0.02 $Å^{-3}$ was used.

We move now to two directions by changing either Li to Na or 12C4 to 15C5. Recall that the lithium atom sits in the middle of the crown-ether in Li(15C5), but Na is further from the ring: M-X distances for Na(12C4) vs. Li(12C4) are 2.52 vs. 0.98 Å; see Table 1. Comparing the Dyson orbitals of Li(12C4), Li(15C5) and Na(12C4), we see that the *sp*-hybridization found for Li(12C4) is not as evident for the latter two systems. Before the *d*-type orbitals, in the Li(15C5) case there are clearly one *s*-type and three *p*-type orbitals (62a through 65a orbitals of Figure S6 of ESI), while in the Na(12C4) case there are two *s*-type and three *p*-type orbitals ($19a_1$, $14b_1$, $14b_2$, $20a_1$, $21a_1$ orbitals of Figure S7 of ESI). In the case of Li(15C5) the excitation energies for the first three excited states drop significantly (from 0.589-0.760 eV to 0.135-0.280 eV; see Table 4). On the other hand, the excitation energies for the first three states of Na(12C4) are larger (1.367-1.858 eV; see Table 4). The first two states have an electron in the outer p_x and p_y orbitals and lie at 1.367

and 1.422 eV. The corresponding values for Li(12C4) are 0.657 and 0.760 eV. Although the excitation energies for Na(12C4) increased, they are still lower than the $3s^1 \rightarrow 3p^1$ excitation of atomic Na (2.103 eV),[113] as happened for Li(12C4) vs. Li.

Overall, Li(15C5) is an outlier and follows closely the shell model of metal ammonia complexes (1s, 1p, 1d, 1f, 2s). Recall that it is the only system with the metal in the center of the crown-ether ring. The rest of the complexes follow the same pattern as Li(12C4): Two of the lowest four excited states having one electron on the p_x and p_y orbitals, and the rest two populate the two sp_z hybrids called sp_z-1 and sp_z-2 in Table 4. Within the sodium and potassium series the p_x and p_y states are degenerate within 0.1 eV (average energy difference = 0.05 eV), and they stabilize (lower excitation energy) as the size of the ring increases. The two sp_z states also stabilize with increasing ring size but their energy difference is always higher than 0.18 eV (average energy difference = 0.27 eV). Finally, the *d*-type states follow a similar pattern. The larger the ring, the lower the excitation energies. Going from Li to Na, the excitation energies increase but they drop again from Na to K. The outlier Li(15C5) structure bears the smallest values.

Table 4. P3+ vertical excitation energies for the lowest lying excited states occupying the p_x, p_y, sp_z-1, sp_z-2, and *d*-type orbitals of the metal crown-ether species. The excitation energy for the valence-s to the valence-p, *p*(M), and lowest energy *d*, *d*(M), atomic orbital for the metal is also listed.

Species	p_x	p_y	sp_z-1 [a]	sp_z-2 [b]	*d* [c]
Li(12C4)	0.657	0.760	0.589	1.032	1.109-1.359
Li(15C5)	0.135	0.280	0.249	N/A	0.592-0.661
Na(12C4)	1.367	1.422	1.858	2.108	2.177-2.280
Na(15C5)	0.848	0.918	0.807	1.157	1.224-1.511
Na(18C6)	0.741	0.741	0.706	0.949	1.062-1.284
K(12C4)	1.012	1.072	1.524	1.704	1.771-1.942
K(15C5)	0.766	0.860	0.926	1.229	1.245-1.520
K(18C6)	0.691	0.691	0.751	1.031	1.031-1.057

[a] Lower energy sp_z hybrid. For Li(12C4) it is polarized towards Li, for Na(12C4) it is nearly isotropic, and for the rest complexes it is polarized towards the crown-ether ring. For Li(15C5) is it a pure p_z orbital.

[b] Higher energy sp_z hybrid. For Li(12C4) it is polarized towards the crown-ether ring, for Na(12C4) it is nearly non-polarized, for Li(15C5) is not existent, and for the rest complexes it is polarized towards the metal center.

[c] Energy range for all five components.

M(12C4)$_2$. In order to identify metal-crown ether sandwich-type complexes, we optimized the structure of a metal interacting with two of the smallest rings (12C4). For all three metals (Li, Na, K) the second crown ether in the global minimum attaches to the metal with a single oxygen atom [lateral or L-K(C12C4)$_2$]. Only for potassium we were able to locate a sandwich-type K(12C4)$_2$ complex [S-K(12C4)$_2$] (see Figure 5 for both isomers) 5.4 kcal/mol higher. Our findings suggest that larger metals tend to favor sandwich systems observed in electrides experimentally, and the formation of electrides as an aggregate of sandwich complexes is possibly driven by the interaction of neighboring units.

The excitation energies for the low-lying electronic states of the S-K(12C4)$_2$ isomer with various EPT methods are listed in Table S22 of ESI. The P3+ excitation energies along with the contours of the corresponding occupied orbital in each electronic state [Dyson orbital for the S-K(12C4)$_2^+$ + e$^-$ → S-K(12C4)$_2$] are shown in Figure 6. The cylindrically symmetric (D_{2d} point group) fully coordinated metal-crown ether complexes adopt a completely different pattern from the pseudo-spherical metal-ammonia or metal-diamine complexes. The ground state is a σ-type orbital ($1a_1$) followed by π-type (1e) at 0.64 eV. The second σ-orbital ($2a_1$) with an additional radial node comes next at 1.06 eV. As happens for the 2*s* of K(12C4), the $2a_1$ (2σ) of S-K(12C4)$_2$ precedes the *d*- or δ-type orbitals ($1b_2$ and $1b_1$ of Figure 6). The lowest energy δ-type state (populating the $1b_1$ and $1b_2$ orbitals) is at 1.15 eV.

The next state corresponds to a p_z-type orbital ($2b_2$; z axis is running through the metal and the centers of the two rings) lying 0.67 eV higher (double excitation energy) than its relative $2p_{x,y}$ (1e) orbitals. The corresponding energy difference for K(en)$_2$ is 0.26 eV (see Table 2) and practically zero for metal ammonia complexes.[58, 59] The 2e and $3a_1$ orbitals (1.43 and 1.52 eV) complete the group of *d*-type states (along with $1b_2$ and $1b_1$), which lie within 0.37 eV, while 3e

corresponds to the second π-type orbital. Finally, the *f*-type orbitals ($1a_2$, 4e, $4a_1$, $4b_2$, 5e) reside within only 0.13 eV indicating that the outer electrons at this energy level are located far enough to experience the structure of the complex as quasi-spherical.

The different pattern of electronic states of S-K(12C4)$_2$ and K(en)$_2$ or other metal-ammonia complexes suggests that the electronic band structure of electrides and liquid metals should be completely different affecting the electronic and magnetic properties of the systems.

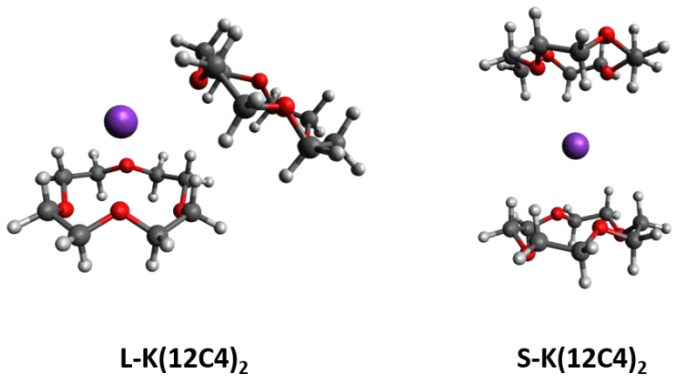

Figure 5. The two located CAM-B3LYP structures for K(12C4)$_2$. The S-K(12C4)$_2$ isomer is higher in energy than L-K(12C4)$_2$ by 5.4 kcal/mol.

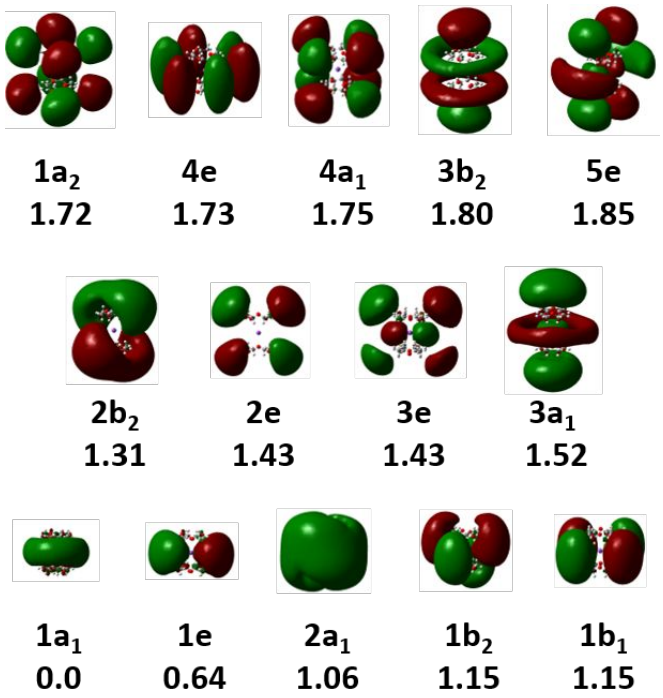

Figure 6. Select Dyson orbitals for the S-K(12C4)$_2^+$ + e$^-$ → S-K(12C4)$_2$ process. An iso-value of 0.005 Å^{-3} was used. The numbers at the bottom of each orbital correspond to vertical excitation energies in eV.

4. Conclusions

High-level electronic structure calculations are performed on metal ethylenediamine, mono- and di-CE complexes. Ground and excited electronic states were examined by means of EPT and large basis sets. Metal ethylenediamine complexes keep the same shell model (1s, 1p, 1d, 2s, 1f) as the metal ammonia complexes but the degeneracy of same-shell orbitals is lifted, and the excitation energies drop due to the screening of the metal charge by the carbon chains. The replacement of ammonia with ethylenediamines affects the stability of the complex by decreasing each metal-nitrogen bond energy by 2.5 kcal/mol.

The ground state of metal mono-CE complexes is formed by the polarization of the valence s-orbital of the alkali metal and the interaction of the positively charged end of the metal with the oxygens of the CE. The excited states do not follow the electronic structure of the atom. Instead, they adopt a similar (to metal ammonia complexes) shell model, but with the 2s being lower in energy and hybridizing with one of the 1p orbitals. For sodium and potassium complexes, the excitation energies drop with the size of the ring or the metal. In all studied complexes, the metal lies out of the CE ring plane except for Li(15C5) complex, where lithium resides in the middle of the ring. This situation affects largely the electronic structure of Li(15C5), which adopts the 1s, 1p, 1d, 1f, 2s pattern, like metal ammonia but 2s is higher in energy.

The second 12C4 ring attaches to the metal with one of its oxygen atoms and only $K(12C4)_2$ has a low-lying sandwich complex justifying why large crowns are necessary for the formation of electrides. For the sandwich complex we calculated excitation energies and showed the thoroughly different shell model for the outer diffuse electrons compared to metal ammonia complexes, partly due to the cylindrical symmetry. Our results suggest that despite the similarity of metal-ammonia and metal-crown ether in the ground state (diffuse s-orbitals), their excited states are completely

different and the electronic properties (such as band structure) of their "polymers" (electrides vs. expanded metals) are expected to differ considerably.

Acknowledgements

The authors are indebted to Auburn University (AU) for financial support. This work was completed with resources provided by the Auburn University Hopper Cluster, Alabama Supercomputer Center, and National Energy Research Scientific Computing Center a DOE Office of Science User Facility supported by the Office of Science of the U.S. Department of Energy under Contract No. DE-AC02-05CH11231. IRA thank Auburn University for the financial assistance through Harry Merriwether Fellowship. We are grateful to Professor J. V. Ortiz, Auburn University, for the valuable discussions that triggered this work. This material is based upon work supported by the National Science Foundation under Grant No. CHE-1940456. Any opinions, findings, and conclusions or recommendations expressed in this material are those of the author(s) and do not necessarily reflect the views of the National Science Foundation.

References

1. C. Liu, S. A. Nikolaev, W. Ren and L. A. Burton, *Journal of Materials Chemistry C*, 2020, **8**, 10551-10567.
2. J. L. Dye, *Science*, 2003, **301**, 607.
3. S. B. Dawes, D. L. Ward, R. H. Huang and J. L. Dye, *J. Am. Chem. Soc.*, 1986, **108**, 3534-3535.
4. A. Ellaboudy, J. L. Dye and P. B. Smith, *J. Am. Chem. Soc.*, 1983, **105**, 6490-6491.
5. R. H. Huang, M. K. Faber, K. J. Moeggenborg, D. L. Ward and J. L. Dye, *Nature*, 1988, **331**, 599-601.
6. S. B. Dawes, J. L. Eglin, K. J. Moeggenborg, J. Kim and J. L. Dye, *J. Am. Chem. Soc.*, 1991, **113**, 1605-1609.
7. R. H. Huang, M. J. Wagner, D. J. Gilbert, K. A. Reidy-Cedergren, D. L. Ward, M. K. Faber and J. L. Dye, *J. Am. Chem. Soc.*, 1997, **119**, 3765-3772.
8. Q. Xie, R. H. Huang, A. S. Ichimura, R. C. Phillips, W. P. Pratt and J. L. Dye, *J. Am. Chem. Soc.*, 2000, **122**, 6971-6978.
9. M. Y. Redko, J. E. Jackson, R. H. Huang and J. L. Dye, *J. Am. Chem. Soc.*, 2005, **127**, 12416-12422.
10. M. J. Wagner, R. H. Huang, J. L. Eglin and J. L. Dye, *Nature*, 1994, **368**, 726-729.
11. Y. Toda, Y. Kubota, M. Hirano, H. Hirayama and H. Hosono, *ACS Nano*, 2011, **5**, 1907-1914.
12. X. Zhang and G. Yang, *J. Phys. Chem. Lett.*, 2020, **11**, 3841-3852.

13. K. Lee, S. W. Kim, Y. Toda, S. Matsuishi and H. Hosono, *Nature*, 2013, **494**, 336-340.
14. Y. Ammari and E. K. Hlil, *Chem. Papers*, 2021, DOI: 10.1007/s11696-021-01543-9.
15. X. Yang, K. Parrish, Y.-L. Li, B. Sa, H. Zhan and Q. Zhu, *Phys. Rev. B*, 2021, **103**, 125103.
16. Y. Toda, H. Hirayama, N. Kuganathan, A. Torrisi, P. V. Sushko and H. Hosono, *Nature Comm.*, 2013, **4**, 2378.
17. M. Kitano, Y. Inoue, Y. Yamazaki, F. Hayashi, S. Kanbara, S. Matsuishi, T. Yokoyama, S.-W. Kim, M. Hara and H. Hosono, *Nature Chem.*, 2012, **4**, 934-940.
18. Y. Kobayashi, M. Kitano, S. Kawamura, T. Yokoyama and H. Hosono, *Catal. Sci. & Tech.*, 2017, **7**, 47-50.
19. H. Buchammagari, Y. Toda, M. Hirano, H. Hosono, D. Takeuchi and K. Osakada, *Org. Lett.*, 2007, **9**, 4287-4289.
20. T.-N. Ye, J. Li, M. Kitano, M. Sasase and H. Hosono, *Chem. Sci.*, 2016, **7**, 5969-5975.
21. E. R. Johnson, A. Otero-de-la-Roza and S. G. Dale, *Journal Chem. Phys.*, 2013, **139**, 184116.
22. S. G. Dale, A. Otero-de-la-Roza and E. R. Johnson, *Phys. Chem. Chem. Phys.*, 2014, **16**, 14584-14593.
23. S. G. Dale and E. R. Johnson, *Phys. Chem. Chem. Phys.*, 2016, **18**, 27326-27335.
24. S. G. Dale and E. R. Johnson, *Phys. Chem. Chem. Phys.*, 2017, **19**, 27343-27352.
25. S. G. Dale and E. R. Johnson, *Phys. Chem. Chem. Phys.*, 2017, **19**, 12816-12825.
26. S. G. Dale and E. R. Johnson, *J. Phys. Chem. A*, 2018, **122**, 9371-9391.
27. S. G. Dale, A. Otero-de-la-Roza and E. R. Johnson, *J. Phys. Chem. C*, 2018, **122**, 12742-12747.
28. A. Ahmed, M. A. Hashmi and K. Ayub, *J. Molec. Liq.*, 2020, **302**, 112577.
29. M. Valente, S. F. Sousa, A. L. Magalhães and C. Freire, *J. Molec. Model.*, 2011, **17**, 3275-3288.
30. J. W. Steed, *Coord. Chem. Rev.*, 2001, **215**, 171-221.
31. A. K. Singha Deb, P. Sahu, A. Boda, S. M. Ali, K. T. Shenoy and D. Upadhyay, *Phys. Chem. Chem. Phys.*, 2020, **22**, 14682-14693.
32. K. Reuter, S. S. Rudel, M. R. Buchner, F. Kraus and C. von Hänisch, *Chem. Eur. J.*, 2017, **23**, 9607-9617.
33. G. Orcajo, H. Montes-Andrés, J. A. Villajos, C. Martos, J. A. Botas and G. Calleja, *Int. J. Hydrog. Energy*, 2019, **44**, 19285-19293.
34. Y. Zhang, X. Wang, B. Luo and Y. Xia, *Journal of Physical Organic Chemistry*, 2012, **25**, 222-229.
35. A. A. Maarouf, R. A. Nistor, A. Afzali-Ardakani, M. A. Kuroda, D. M. Newns and G. J. Martyna, *J. Chem. Theory and Comput.*, 2013, **9**, 2398-2403.
36. J. Guo, J. Lee, C. I. Contescu, N. C. Gallego, S. T. Pantelides, S. J. Pennycook, B. A. Moyer and M. F. Chisholm, *Nature Comm.*, 2014, **5**, 5389.
37. J. J. Heath and M. A. Kuroda, *Phys. Chem. Chem. Phys.*, 2018, **20**, 25822-25828.
38. M. Gao, Y. Wang, Q. Yi, Y. Su, P. Sun, X. Wang, J. Zhao and G. Zou, *J. Mater. Chem. A*, 2015, **3**, 20541-20546.
39. P. Thuéry, Y. Atoini and J. Harrowfield, *Cryst. Growth & Des.*, 2018, **18**, 3167-3177.
40. N. V. Tkachenko, Z.-M. Sun and A. I. Boldyrev, *ChemPhysChem*, 2019, **20**, 2060-2062.
41. P. P. Edwards, A. R. Lusis and M. J. Sienko, *J. Chem. Phys.*, 1980, **72**, 3103-3112.
42. R. Hagedorn and M. J. Sienko, *J. Phys. Chem.*, 1982, **86**, 2094-2097.
43. A. M. Stacy, D. C. Johnson and M. J. Sienko, *J. Chem. Phys.*, 1982, **76**, 4248-4254.
44. A. M. Stacy and M. J. Sienko, *Inorg. Chem.*, 1982, **21**, 2294-2297.
45. Y. Nakamura, M. Niibe and M. Shimoji, *J. Phys. Chem.*, 1984, **88**, 3755-3760.
46. J. Kohanoff, F. Buda, M. Parrinello and M. L. Klein, *Phys. Rev. Lett.*, 1994, **73**, 3133-3136.
47. S. Hayama, J. C. Wasse, N. T. Skipper and A. K. Soper, *J. Phys. Chem. B*, 2002, **106**, 11-14.
48. H. Thompson, J. C. Wasse, N. T. Skipper, S. Hayama, D. T. Bowron and A. K. Soper, *J. Am. Chem. Soc.*, 2003, **125**, 2572-2581.

49. R. M. Ibberson, A. J. Fowkes, M. J. Rosseinsky, W. I. F. David and P. P. Edwards, *Angew. Chem. Int. Ed.*, 2009, **48**, 1435-1438.
50. E. Zurek, P. P. Edwards and R. Hoffmann, *Angew. Chem. Int. Ed.*, 2009, **48**, 8198-8232.
51. K. Maeda, M. T. J. Lodge, J. Harmer, J. H. Freed and P. P. Edwards, *J. Am. Chem. Soc.*, 2012, **134**, 9209-9218.
52. A. G. Seel, E. Zurek, A. J. Ramirez-Cuesta, K. R. Ryan, M. T. J. Lodge and P. P. Edwards, *Chem. Comm.*, 2014, **50**, 10778-10781.
53. P. P. Edwards, *J. Supercond.*, 2000, **13**, 933-946.
54. T. A. Kaplan, J. F. Harrison, J. L. Dye and R. Rencsok, *Phys. Rev. Lett.*, 1995, **75**, 978-978.
55. N. M. S. Almeida and E. Miliordos, *Phys. Chem. Chem. Phys.*, 2019, **21**, 7098-7104.
56. N. M. S. Almeida, F. Pawłowski, J. V. Ortiz and E. Miliordos, *Phys. Chem. Chem. Phys.*, 2019, **21**, 7090-7097.
57. S. N. Khan and E. Miliordos, *The Journal of Physical Chemistry A*, 2020, **124**, 4400-4412.
58. I. R. Ariyarathna, S. N. Khan, F. Pawłowski, J. V. Ortiz and E. Miliordos, *J. Phys. Chem. Lett.*, 2018, **9**, 84-88.
59. I. R. Ariyarathna, F. Pawłowski, J. V. Ortiz and E. Miliordos, *Phys. Chem. Chem. Phys.*, 2018, **20**, 24186-24191.
60. I. R. Ariyarathna, N. M. S. Almeida and E. Miliordos, *J. Phys. Chem. A*, 2019, **123**, 6744-6750.
61. I. R. Ariyarathna and E. Miliordos, *Phys. Chem. Chem. Phys.*, 2019, **21**, 15861-15870.
62. I. R. Ariyarathna and E. Miliordos, *Phys. Chem. Chem. Phys.*, 2020, **22**, 22426-22435.
63. I. R. Ariyarathna and E. Miliordos, *J. Phys. Chem. A*, 2020, **124**, 9783-9792.
64. I. R. Ariyarathna, F. Pawłowski, J. V. Ortiz and E. Miliordos, *J. Phys. Chem. A*, 2020, **124**, 505-512.
65. B. A. Jackson and E. Miliordos, *J. Chem. Phys.*, 2021.
66. I. R. Ariyarathna and E. Miliordos, *Int. J. Quantum Chem.*, 2018, **118**, e25673.
67. W. D. Knight, K. Clemenger, W. A. de Heer, W. A. Saunders, M. Y. Chou and M. L. Cohen, *Phys. Rev. Lett.*, 1984, **52**, 2141-2143.
68. M. G. J. Mayer, J. H. D., *Elementary Theory of Nuclear Structure*, Wiley, New York, 1955.
69. A. H. C. West, B. L. Yoder, D. Luckhaus, C.-M. Saak, M. Doppelbauer and R. Signorell, *J. Phys. Chem. Lett.*, 2015, **6**, 1487-1492.
70. S. Hartweg, A. H. C. West, B. L. Yoder and R. Signorell, *Angew. Chem. Int. Ed.*, 2016, **55**, 12347-12350.
71. T. E. Gartmann, B. L. Yoder, E. Chasovskikh and R. Signorell, *Chem. Phys. Lett.*, 2017, **683**, 515-520.
72. J. V. Barnes, B. L. Yoder and R. Signorell, *J. Phys. Chem. A*, 2019, **123**, 2379-2386.
73. B. M. Reinhard and G. Niedner-Schatteburg, *Phys. Chem. Chem. Phys.*, 2002, **4**, 1471-1477.
74. B. M. Reinhard and G. Niedner-Schatteburg, *J. Chem. Phys.*, 2003, **118**, 3571-3582.
75. B. M. Reinhard and G. Niedner-Schatteburg, *Phys. Chem. Chem. Phys.*, 2003, **5**, 1970-1980.
76. W. J. Glover, R. E. Larsen and B. J. Schwartz, *J. Phys. Chem. B*, 2010, **114**, 11535-11543.
77. A. G. Seel, H. Swan, D. T. Bowron, J. C. Wasse, T. Weller, P. P. Edwards, C. A. Howard and N. T. Skipper, *Angew. Chem. Int. Ed.*, 2017, **56**, 1561-1565.
78. I. R. Ariyarathna, *Phys. Chem. Chem. Phys.*, 2021, **23**, 16206-16212.
79. I. R. Ariyarathna, *Phys. Chem. Chem. Phys.*, 2021, DOI: 10.1039/D1CP03146E.
80. I. R. Ariyarathna, *Int. J. Quantum Chem.*, 2021, **n/a**, e26774.
81. A. H. C. West, B. L. Yoder, D. Luckhaus and R. Signorell, *J. Phys. Chem. A*, 2015, **119**, 12376-12382.
82. J. V. Barnes, M. Beck, S. Hartweg, A. Luski, B. L. Yoder, J. Narevicius, E. Narevicius and R. Signorell, *Phys. Chem. Chem. Phys.*, 2021, **23**, 846-858.
83. T. Buttersack, P. E. Mason, R. S. McMullen, H. C. Schewe, T. Martinek, K. Brezina, M. Crhan, A. Gomez, D. Hein, G. Wartner, et al., *Science*, 2020, **368**, 1086.
84. A. O. Gunina and A. I. Krylov, *J. Phys. Chem. A*, 2016, **120**, 9841-9856.

85. M. V. Ivanov, A. I. Krylov and S. Zilberg, *J. Phys. Chem. Lett.*, 2020, **11**, 2284-2290.
86. P. E. Mason, H. C. Schewe, T. Buttersack, V. Kostal, M. Vitek, R. S. McMullen, H. Ali, F. Trinter, C. Lee, D. M. Neumark, et al., *Nature*, 2021, **595**, 673-676.
87. C. Møller and M. S. Plesset, *Phys. Rev.*, 1934, **46**, 618-622.
88. K. Raghavachari, G. W. Trucks, J. A. Pople and M. Head-Gordon, *Chem. Phys. Lett.*, 1989, **157**, 479-483.
89. P. J. Knowles, C. Hampel and H. J. Werner, *J. Chem. Phys.*, 1993, **99**, 5219-5227.
90. J. D. Watts, J. Gauss and R. J. Bartlett, *J. Chem. Phys.*, 1993, **98**, 8718-8733.
91. P. J. Knowles, C. Hampel and H.-J. Werner, *J. Chem. Phys.*, 2000, **112**, 3106-3107.
92. P. Hohenberg and W. Kohn, *Phys. Rev.*, 1964, **136**, B864-B871.
93. W. Kohn and L. J. Sham, *Phys. Rev.*, 1965, **140**, A1133-A1138.
94. T. H. Dunning, *J. Chem. Phys.*, 1989, **90**, 1007-1023.
95. B. P. Prascher, D. E. Woon, K. A. Peterson, T. H. Dunning and A. K. Wilson, *Theor. Chem. Acc.*, 2011, **128**, 69-82.
96. *The K basis sets were provided by Professor Kirk Peterson (washington State University); private communication.*
97. R. A. Kendall, T. H. Dunning and R. J. Harrison, *J. Chem. Phys.*, 1992, **96**, 6796-6806.
98. T. Koopmans, *Physica*, 1934, **1**, 104-113.
99. J. V. Ortiz, *Int. J. Quantum Chem.*, 2005, **105**, 803-808.
100. J. V. Ortiz, *WIREs Computational Molecular Science*, 2013, **3**, 123-142.
101. H. H. Corzo and J. V. Ortiz, in *Advances in Quantum Chemistry*, eds. J. R. Sabin and E. J. Brändas, Academic Press, 2017, vol. 74, pp. 267-298.
102. J. F. Stanton and J. Gauss, *J. Chem. Phys.*, 1994, **101**, 8938-8944.
103. M. Nooijen and R. J. Bartlett, *J. Chem. Phys.*, 1995, **102**, 3629-3647.
104. A. I. Krylov, *Ann. Rev. Phys. Chem.*, 2008, **59**, 433-462.
105. R. J. Bartlett, *WIREs Comput. Molec. Sci.*, 2012, **2**, 126-138.
106. D. E. Woon and T. H. Dunning, *J. Chem. Phys.*, 1994, **100**, 2975-2988.
107. M. J. Frisch, G. W. Trucks, H. B. Schlegel, G. E. Scuseria, M. A. Robb, J. R. Cheeseman, G. Scalmani, V. Barone, G. A. Petersson, H. Nakatsuji, et al. *Gaussian 16 Rev. C.01*, Wallingford, CT, 2016.
108. H.-J. Werner, P. J. Knowles, G. Knizia, F. R. Manby, M. {Schütz}, P. Celani, W. Györffy, D. Kats, T. Korona, R. Lindh, et al. *MOLPRO, version 2015.1, a package of ab initio programs*, 2015.
109. Y. Shao, Z. Gan, E. Epifanovsky, A. T. B. Gilbert, M. Wormit, J. Kussmann, A. W. Lange, A. Behn, J. Deng, X. Feng, et al., *Molec. Phys.*, 2015, **113**, 184-215.
110. G. Schaftenaar and J. H. Noordik, *J. Comput. Aided Mol. Des.*, 2000, **14**, 123-134.
111. G. Schaftenaar, E. Vlieg and G. Vriend, *J. Comput. Aided Mol. Des.*, 2017, **31**, 789-800.
112. R. Dennington, T. A. Keith and J. M. Millam *GaussView, Version 6.1*, Semichem Inc.: Shawnee Mission, KS, 2016.
113. W. M. Haynes, *CRC Handbook of Chemistry and Physics, 93rd Edition*, Taylor & Francis, 2012.
114. I. R. Ariyarathna, Ph.D. thesis, Auburn University, 2021.